


## First-principles quantum Monte Carlo study of charge-carrier mobility in organic molecular semiconductors

Johann Ostmeyer<sup>1,\*</sup>, Tahereh Nemataram<sup>2</sup>, Alessandro Troisi<sup>3</sup>, and Pavel Buividovich<sup>1</sup>

<sup>1</sup>Department of Mathematical Sciences, University of Liverpool, Liverpool, United Kingdom

<sup>2</sup>Department of Pure and Applied Chemistry, University of Strathclyde, Glasgow, United Kingdom

<sup>3</sup>Department of Chemistry, University of Liverpool, Liverpool, United Kingdom

 (Received 5 January 2024; revised 29 May 2024; accepted 13 August 2024; published 10 September 2024)

We present a first-principles numerical study of charge transport in a realistic two-dimensional tight-binding model of organic molecular semiconductors. We use the hybrid Monte Carlo (HMC) algorithm to simulate the full quantum dynamics of phonons and either single or multiple charge carriers without any tunable parameters. We introduce a number of algorithmic improvements, including efficient Metropolis updates for phonon fields based on analytical insights, which lead to negligible autocorrelation times and allow sub-per-mille precisions to be reached at a low computational cost of  $\mathcal{O}(1)$  CPU hours. Our simulations produce charge-mobility estimates that are in good agreement with experiments and that also justify the phenomenological transient localization approach.

DOI: [10.1103/PhysRevApplied.22.L031004](https://doi.org/10.1103/PhysRevApplied.22.L031004)

*Introduction.* Organic molecular semiconductors are technologically interesting materials with distinctive charge-transport physics [1]. The conduction and valence bands are narrow and can be described as being formed by the highest occupied and lowest unoccupied molecular orbitals of the constituent molecules. The transfer integrals between these localized orbitals undergo large thermal fluctuations, similar in magnitude to the transfer integrals themselves. With characteristic optical phonon frequencies being considerably smaller than both the temperature and the bandwidth, the resulting dynamic disorder has been extensively studied using semiclassical approaches to nuclear degrees of freedom, such as Ehrenfest dynamics [2] or surface hopping [3–6]. These studies led to the conjecture of an unconventional transient localization (TL) charge-transport mechanism [7,8], driven by transitions between electron states that are transiently localized (in the Anderson sense) at timescales shorter than inverse characteristic phonon frequencies [9–15].

However, it is well known that semiclassical approximations for nuclear degrees of freedom (or, equivalently, phonons) may lead to incorrect conclusions about charge transport in the case of strong electron-phonon interactions [16,17]. To ensure that the popular TL scenario is not an artefact of semiclassical approximations, it is therefore

extremely important to verify it in first-principles simulations without any assumptions about the classical behavior of phonons or nuclei.

So far, first-principles numerical studies of charge transport in molecular semiconductors were carried out only for one-dimensional models, mostly at low charge density [18–21] (see Ref. [22] for an overview of relevant numerical methods). However, the dimensionality of the model has dramatic effects on the physics involving disorder-driven localization in the electronic Hamiltonian. The vast majority of molecular semiconductors have a layered structure, such that transport takes place predominantly in a two-dimensional (2D) plane. It is also observed that a fairly general model that captures almost the entire class of crystalline materials is formed by molecules on a triangular lattice interacting with their three nonequivalent neighbors through a transfer integral that is (heavily) modulated by phonons, see Fig. 1. This class of materials is well described by the TL model in the relaxation-time approximation (RTA) [23], also in the presence of high-frequency phonons that effectively renormalize the bandwidth [12]. However, the corresponding relaxation time,  $\tau_{\text{in}}$ , is a phenomenological parameter that is not directly connected to the model Hamiltonian and cannot be assumed to be universal.

Here, we propose hybrid Monte Carlo (HMC) simulations of the two-dimensional tight-binding model on a triangular lattice as a first-principles reference methodology to describe charge transport in molecular semiconductors. We calculate the charge-carrier mobility and its temperature dependence entirely from first principles for a broad range of model parameters, without possible artefacts from considering the nuclei classically [2–5],

\*Contact author: [ostmeyer@hiskp.uni-bonn.de](mailto:ostmeyer@hiskp.uni-bonn.de)

Published by the American Physical Society under the terms of the [Creative Commons Attribution 4.0 International](https://creativecommons.org/licenses/by/4.0/) license. Further distribution of this work must maintain attribution to the author(s) and the published article's title, journal citation, and DOI.

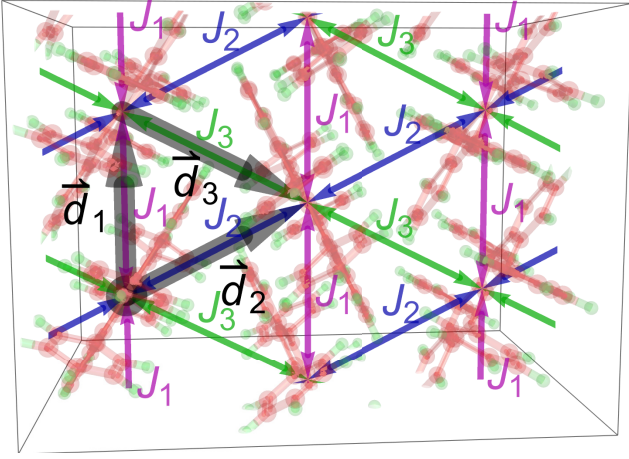


FIG. 1. Triangular lattice structure of a rubrene crystal, a representative organic molecular semiconductor, in the high-mobility plane with transfer integrals ( $J_a$ ) and lattice vectors ( $\vec{d}_a$ ) for each lattice bond.

introducing phenomenological quantities such as the relaxation time [23], or neglecting interelectron interactions at high charge densities. The only inputs are the parameters of the 2D tight-binding Hamiltonian, such as intermolecular transfer integrals, optical phonon frequencies, and phonon coupling strengths, which are the direct outputs of the electronic structure calculations [13].

*Tight-binding model and imaginary-time path integral formulation.* We follow Ref. [23] and model the wide class of crystalline molecular semiconductors in terms of the two-dimensional tight-binding Hamiltonian describing charge carriers (holes) interacting with dispersionless phonons on an anisotropic triangular lattice:

$$\hat{\mathcal{H}} = \sum_{k,a} \left( \frac{\hat{p}_{k,a}^2}{2} + \frac{\omega_0^2 \hat{x}_{k,a}^2}{2} \right) - \mu_e \sum_{k,s} \hat{c}_{k,s}^\dagger \hat{c}_{k,s} - \sum_{k,a,s} J_a (1 - \lambda_a \hat{x}_{k,a}) \left( \hat{c}_{k,s}^\dagger \hat{c}_{k+\bar{a},s} + \hat{c}_{k+\bar{a},s}^\dagger \hat{c}_{k,s} \right), \quad (1)$$

$$\equiv \hat{\mathcal{H}}_{\text{ph}}(\hat{x}, \hat{p}) + \sum_{k,l,s} \hat{c}_{k,s}^\dagger (H_{kl}[\hat{x}] - \mu_e \delta_{kl}) \hat{c}_{l,s}, \quad (2)$$

where the indices  $k, l$  label sites of a triangular lattice;  $\hat{c}_{k,s}^\dagger, \hat{c}_{k,s}$  are the creation and annihilation operators for a charge carrier with spin  $s$ ;  $a$  enumerates three (forward) directions of lattice bonds between nearest-neighbor sites  $k$  and  $k + \bar{a}$ ;  $J_a$  are the corresponding charge-transfer integrals;  $\lambda_a$  are the electron-phonon coupling constants; and  $\mu_e$  is the chemical potential. We assume periodic boundary conditions. Phonons with frequency  $\omega_0$  are associated with lattice bonds and described by a quadratic Hamiltonian,  $\hat{\mathcal{H}}_{\text{ph}}$ , with amplitudes  $\hat{x}_{k,a}$  and momenta  $\hat{p}_{k,a}$ . We also introduce a single-particle Hamiltonian,  $H_{kl}[\hat{x}]$ , in the

background of phonon fields  $\hat{x}_{k,a}$ . We do not consider electrostatic interactions between charge carriers, which are negligible at low concentrations.

Our HMC simulations at finite temperature  $T$  are based on the standard representation of the thermal partition function,  $\mathcal{Z} = \text{Tr} e^{-\beta \hat{\mathcal{H}}}$ ,  $\beta \equiv T^{-1}$ , in terms of the path integral  $\int \mathcal{D}x_{k,a}(\tau)$  over all possible configurations of phonon fields  $x_{k,a}(\tau)$  on a finite interval of Euclidean (imaginary) time  $\tau \in [0, \beta]$  with periodic boundary conditions  $x_{k,a}(0) \equiv x_{k,a}(\beta)$  [24,25]:

$$\mathcal{Z} = \int \mathcal{D}x_{k,a}(\tau) \exp(-S_{\text{ph}}[x(\tau)]) \times \det \left( 1 + e^{\beta \mu_e} \mathcal{T} e^{-\int_0^\beta d\tau H[x(\tau)]} \right)^{N_s}, \quad (3)$$

where  $\mathcal{T} e^{(\dots)}$  is a time-ordered exponent. The Euclidean action,  $S_{\text{ph}}[x(\tau)]$ , for phonons is

$$S_{\text{ph}}[x(\tau)] = \int_0^\beta d\tau \left( \frac{1}{2} \left( \frac{dx_{k,a}(\tau)}{d\tau} \right)^2 + \frac{\omega_0^2 x_{k,a}^2(\tau)}{2} \right).$$

The argument for the determinant in Eq. (3) is a real-valued matrix for any chemical potential  $\mu_e$ , which implies that the path integral weight is real and non-negative for  $N_s = 2$  spin components and any chemical potential  $\mu_e$ . Correspondingly, it can be used as a statistical weight for Monte Carlo algorithms, which generate configurations of phonon fields  $x_{i,a}(\tau)$  with probability proportional to the integrand of Eq. (3). Technical details of the derivations and numerical algorithms are provided in the Supplemental Material [26].

*Mobility calculations.* The charge mobility,  $\mu$ , is calculated as the ratio of  $\mu = \sigma(\omega \rightarrow 0)/n$  of the zero-frequency limit of the ac electrical conductivity,  $\sigma(\omega)$ , to the charge density,  $n = \langle \hat{c}_{k,s}^\dagger \hat{c}_{k,s} \rangle \equiv \mathcal{Z}^{-1} \text{Tr} \left( e^{-\beta \hat{\mathcal{H}}} \hat{c}_{k,s}^\dagger \hat{c}_{k,s} \right)$ . The conductivity,  $\sigma(\omega)$ , is defined in terms of the full Cartesian conductivity tensor as  $\sigma(\omega) = (\sigma_{xx}(\omega) + \sigma_{yy}(\omega))/2$ . We follow the standard approach in quantum Monte Carlo simulations [18,19,27,28] and extract the conductivity from imaginary-time correlators of electric currents:

$$G(\tau) = \frac{1}{2\mathcal{Z}} \sum_{\alpha=x,y} \text{Tr} \left( \hat{\mathcal{I}}_\alpha e^{-\tau \hat{\mathcal{H}}} \hat{\mathcal{I}}_\alpha e^{-(\beta-\tau) \hat{\mathcal{H}}} \right). \quad (4)$$

Here, the electric current operator,  $\hat{\mathcal{I}}_\alpha$ , is defined as

$$\hat{\mathcal{I}}_\alpha = i \sum_{k,s,a} (d_a)_\alpha J_a (1 - \lambda_a \hat{x}_{k,a}) \left( \hat{c}_{k+\bar{a},s}^\dagger \hat{c}_{k,s} - \hat{c}_{k,s}^\dagger \hat{c}_{k+\bar{a},s} \right),$$

where  $(d_a)_\alpha$ ,  $\alpha = x, y$  are the Cartesian vectors of the lattice bonds in direction  $a$ . We represent the correlator, Eq. (4), as a convolution of single-particle fermionic

Green's functions, which are averaged over phonon fields  $x_{k,a}(\tau)$ .

The electrical conductivity,  $\sigma(\omega)$ , is finally estimated by inverting the Green-Kubo relationship,

$$G(\tau) = \int_0^{+\infty} \frac{d\omega}{\pi} \frac{\omega \cosh(\omega(\tau - \beta/2))}{\sinh(\omega\beta/2)} \sigma(\omega), \quad (5)$$

using the Backus-Gilbert method [28–30].

*Monte carlo algorithm.* To sample phonon fields  $x_{k,a}(\tau)$  with a probability distribution that corresponds to the path integral weight in Eq. (3), we use the HMC algorithm [31–33] with an exact Fourier acceleration (EFA) [34] inspired by Refs. [35–37] that relies on the analytical integration of the bosonic molecular dynamics. The HMC algorithm is universally applicable throughout the entire parameter space of the model, Eq. (1), and for any value of charge density. It provides reliable first-principles estimates of the mobility,  $\mu$ , in a run time that scales as  $\mathcal{O}(V^3) + \mathcal{O}(V^2 N_\tau \ln N_\tau)$ , where  $V$  is the number of lattice sites and  $N_\tau$  is the number of discrete steps in  $\tau$  used to calculate the time-ordered exponent in Eq. (3) [26]. An implementation is publicly available [38].

We find that our HMC algorithm with EFA is extremely efficient over the entire range of experimentally relevant Hamiltonian parameters and temperatures  $T = 100$ – $400$  K and does not suffer from long autocorrelation times [25,26,39], in contrast to previous HMC studies of electron-phonon models [39–42] that focus on spontaneously ordered electron states.

*Low-density or single-charge-carrier limit.* Typical charge densities in molecular semiconductors are very low,  $n \lesssim 0.01$ . As we explicitly demonstrate in Fig. 2, interelectron interactions become negligible at such low densities, and it is sufficient to consider the dynamics of a single charge carrier interacting with a bath of thermal phonons [7,18–20,22]. Therefore, we also consider this regime explicitly, in addition to the full finite-density simulations, which allows us to accelerate our HMC algorithm even further.

Expanding the many-body partition function, Eq. (3), in powers of the fugacity,  $e^{\beta\mu_e}$ , the partition function in the Hilbert subspace with charge  $Q = 1$  is found to be [26]

$$\mathcal{Z}_1 = \int \mathcal{D}x_{k,a}(\tau) e^{-S_{\text{ph}}[x(\tau)]} \text{Tr} \mathcal{T} e^{-\int_0^\beta d\tau H[x(\tau)]}. \quad (6)$$

The path integral weight in Eq. (6) is always positive for our range of model parameters, which allows us to use the HMC algorithm with EFA again. This provides a practical alternative to worldline (WLMC) [19] and diagrammatic Monte Carlo [18] simulations for polaron-type single-particle systems, which becomes particularly advantageous for charge transport in molecular semiconductors. The equivalence between HMC and the ensemble

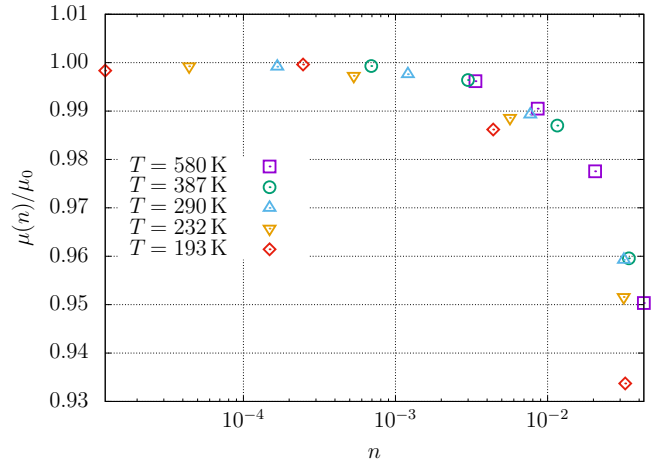


FIG. 2. Ratio of the finite-density charge mobility,  $\mu(n)$ , to its low-density limit,  $\mu_0 = \mu(n \rightarrow 0)$ , as a function of charge density,  $n$ , for a symmetric generic molecular semiconductor with  $J = 100$  meV. See Fig. 4 within the Supplemental Material [26] for the dependence of both quantities on the chemical potential. Errors are smaller than data points [26].

of single-particle worldlines in WLMC simulations is readily established using the hopping expansion of the non-local factor  $\text{Tr} \mathcal{T} e^{-\int_0^\beta d\tau H[x(\tau)]}$ . Within a few CPU hours, the HMC yields the current-current correlator, Eq. (4), in the single-particle Hilbert subspace on lattices with  $\mathcal{O}(1000)$  sites with per-mille-level precision, which is crucial for a numerically stable inversion of the Green-Kubo relationship, Eq. (5).

*Numerical results.* To illustrate the main features of our numerical method and to compare it with the TL approach, we consider a large class of molecular semiconductors (including rubrene, see Fig. 1), which can be mapped onto the tight-binding Hamiltonian, Eq. (1), with  $J_2 = J_3 \neq J_1$  with sufficiently good precision [23]. We use a convenient parametrization [23]:

$$J_1 = J \cos \theta, \quad J_2 = J \sin \theta / \sqrt{2}, \quad J_3 = J \sin \theta / \sqrt{2}. \quad (7)$$

Thermal fluctuations of transfer integrals are usually around  $\Delta J_a \approx J_a/2$  at room temperature,  $T_0 = 25$  meV. From this, we estimate the electron-phonon couplings,  $\lambda_a$  in Eq. (1), and assume that  $\lambda_a$  are temperature independent, so that the temperature dependence of  $\Delta J_a$  is entirely driven by thermal phonon fluctuations,  $\langle \hat{x}_{k,a}^2 \rangle$ . When we consider the parametrization of Eq. (7) for a *generic molecular semiconductor*, we assume a typical triangular lattice with bond lengths  $|\vec{d}_a| = 7.2$  Å (see Fig. 1) and phonon frequencies  $\omega_0 = 6$  meV [1,23,26].

First, we check the range of applicability of the low-density (single-particle) approximation by performing full HMC simulations at finite charge densities and checking how quickly the low-density limit,  $\mu_0 = \mu(n \rightarrow 0)$ , of

mobility is approached. The convergence is visualized in Fig. 2 for a symmetric generic molecular semiconductor with  $J_1 = J_2 = J_3 = 100 \text{ meV}/\sqrt{3}$ . We use lattices with  $15 \times 15$  and  $18 \times 18$  lattice sites, with  $N_\tau = 48$  and  $N_\tau = 64$  steps for Euclidean time  $\tau$  in Eq. (3), thereby explicitly checking that we reach the thermodynamic and continuum-time limits [26]. The results from  $18 \times 18$  lattices with  $N_\tau = 64$  shown in Fig. 2 suggest that finite-density effects become smaller than 1% at  $n \lesssim 0.01$  holes per lattice cell, which is in good correspondence with typical charge densities in transistor devices based on molecular semiconductors. In what follows, we therefore present the mobility values obtained directly at the single-particle (low-density) limit from Eq. (6).

In Fig. 3, we present the temperature dependence of the low-density charge mobility in a generic molecular semiconductor with parametrization, Eq. (7), fitting data to the power law,  $\mu \sim T^{-\alpha}$ ,  $\alpha > 0$ , expected for bandlike transport. The fits describe the data very well, supporting the experimental evidence [4] for an intermediate regime between bandlike transport and thermally activated hopping in molecular semiconductors in the experimentally relevant range of parameters and temperatures. More specifically, close to the symmetric case,  $\theta/\pi \approx 0.3$ , we find  $\alpha = 1$  with very high precision.

As a benchmark of the TL model, in Fig. 4, we compare HMC results for the dependence of charge mobility on the relative magnitude of transfer integrals, as parametrized by  $\theta$  in Eq. (7), with the predictions of TL RTA calculations [23] (with relaxation time  $\tau_{\text{in}} = 1/\omega_0$ , which is typical for this method, but might not be the optimal value [43]). Both methods produce a qualitatively similar dependence on  $\theta$ , but the HMC yields a considerably stronger dependence on the overall hopping strength,  $J$ , towards

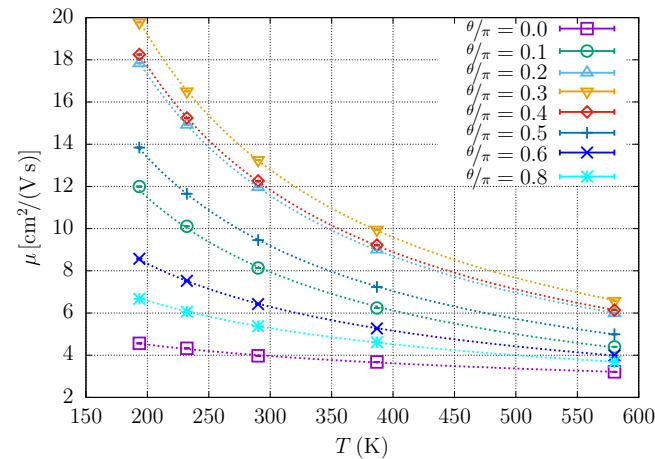


FIG. 3. Temperature dependence of low-density charge mobility in generic molecular semiconductors with different values of  $\theta$ . Dashed lines are fits to the power law,  $\mu \sim T^{-\alpha}$ , with maximal  $\alpha = 1.0(5)$  for the angle region  $0.2 \leq \theta/\pi \leq 0.4$  and a monotonous decrease to  $\alpha = 0.317(8)$  for  $\theta = 0$ .

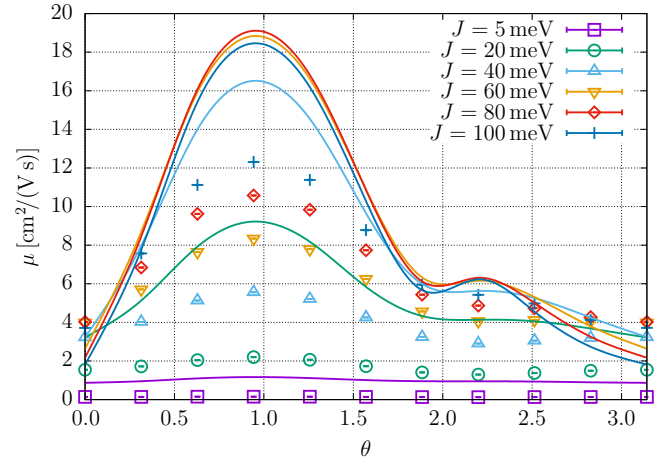


FIG. 4. Dependence of low-density room-temperature charge mobility ( $\mu$ ) of generic molecular semiconductors on the relative magnitudes of transfer integrals, as parametrized by  $\theta$  in Eq. (7) from HMC (points) and TL (lines) calculations.

$J \sim 100 \text{ meV}$ . Both HMC and TL yield maximal mobility for the maximally symmetric case with  $J_1 = J_2 = J_3$ , and minimal for nearly one-dimensional materials with  $J_2 = J_3 = 0$ .

Finally, Fig. 5 shows a comparison of our HMC results with experimental data on charge mobilities for six representative molecular semiconductors (TIPS-Pentacene, C8-DNTT-C8, C8-BTBT, C10-DNTT, rubrene, C10-DNBDT) using exact data for the parameters of the Hamiltonian, Eq. (1) [26]. Transfer integrals,  $J_a$ , with their characteristic fluctuations,  $\Delta J_a$ , are obtained from *ab initio* electronic structure calculations [4,23,44] and lattice structures are taken from the Cambridge Structural Database [45] and Refs. [46–48]. The agreement with experimental data is rather good. Since our methodology is free

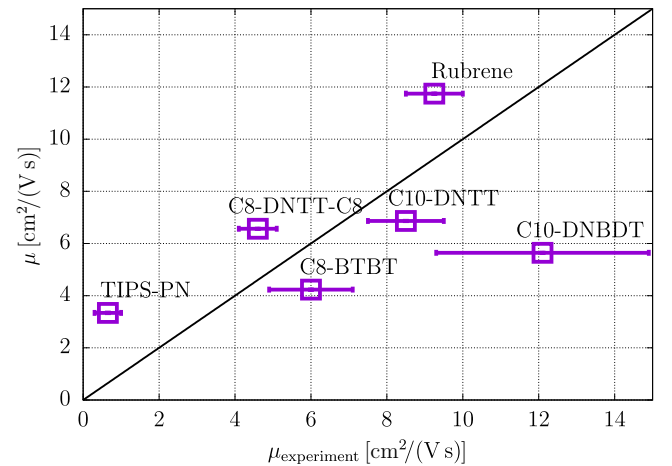


FIG. 5. HMC results for room-temperature charge mobility versus experimental results (from Refs. [4,23,44]) for six representative materials. See the Supplemental Material [26] for details.



of any approximations, given the initial Hamiltonian, any deviations from experiment are either due to experimental uncertainties or limitations of our model Hamiltonian, Eq. (1) (such as a simplified phonon spectrum with just a single frequency).

*Conclusions and outlook.* We advocate HMC simulations as an efficient tool for first-principles studies of charge transport in molecular semiconductors. Its computational efficiency makes the HMC well-suited for the discovery of high-mobility semiconductors by means of large-scale scans through the space of Hamiltonian parameters [13,23]. Our results also provide a rigorous justification of the TL model without invoking any phenomenological parameters, such as relaxation time.

Our numerical approach is ready to be extended towards more realistic simulations. Since the computational complexity of the method is dominated by manipulations with fermionic matrices, additional phonon modes, nontrivial phonon dispersions, and nonlinear terms in the electron-phonon and phonon-phonon interactions can all be introduced practically at no extra cost. Extrinsic disorder, which is important for the realistic description of charge localization at low temperatures,  $T \lesssim 150$  K [19,20], can be easily introduced as a random site-dependent chemical potential in the Hamiltonian, Eq. (1). Likewise, charge-carrier interactions in doped organic semiconductors [49] can be treated by the HMC algorithm without any approximations. The method can also easily accommodate the effects of an external magnetic field, such as the Hall current and spin polarization. Optical response in the THz range is also straightforward to explore.

*Acknowledgments.* We thank Simone Fratini for clarifications of the TL methodology. This work was funded in part by the STFC Consolidated Grant No. ST/T000988/1 and by the Deutsche Forschungsgemeinschaft (DFG, German Research Foundation) as part of the CRC 1639 NuMerIQS – project No. 511713970. A.T. thanks the European Research Council (Grant No. 101020369) for supporting his research. Numerical simulations were undertaken on Barkla, part of the high-performance computing facilities at the University of Liverpool, UK.

- 
- [1] S. Fratini, M. Nikolka, A. Salleo, G. Schweicher, and H. Siringhaus, Charge transport in high-mobility conjugated polymers and molecular semiconductors, *Nat. Mater.* **19**, 491 (2020).
- [2] A. Troisi and G. Orlandi, Charge-transport regime of crystalline organic semiconductors: Diffusion limited by thermal off-diagonal electronic disorder, *Phys. Rev. Lett.* **96**, 086601 (2006).
- [3] S. Giannini, A. Carof, M. Ellis, H. Yang, O. G. Ziogos, S. Ghosh, and J. Blumberger, Quantum localization and delocalization of charge carriers in organic semiconducting crystals, *Nat. Commun.* **10**, 3843 (2019).

- [4] S. Giannini, L. Di Virgilio, M. Bardini, J. Hausch, J. Geuchies, W. Zheng, M. Volpi, J. Elsner, K. Broch, Y. H. Geerts, F. Schreiber, G. Schweicher, H. I. Wang, J. Blumberger, M. Bonn, and D. Beljonne, Transiently delocalized states enhance hole mobility in organic molecular semiconductors, *Nat. Mater.* **22**, 1361 (2023).
- [5] S. Giannini and J. Blumberger, Charge transport in organic semiconductors: The perspective from nonadiabatic molecular dynamics, *Acc. Chem. Res.* **55**, 819 (2022).
- [6] J. E. Runeson, T. J. G. Drayton, and D. E. Manolopoulos, Charge transport in organic semiconductors from the mapping approach to surface hopping, [arXiv:2406.19851](https://arxiv.org/abs/2406.19851).
- [7] S. Fratini, D. Mayou, and S. Ciuchi, The transient localization scenario for charge transport in crystalline organic materials, *Adv. Funct. Mater.* **26**, 2292 (2016).
- [8] H. Rammal, A. Ralko, S. Ciuchi, and S. Fratini, Transient localization from the interaction with quantum bosons, *Phys. Rev. Lett.* **132**, 266502 (2024).
- [9] S. Ciuchi, S. Fratini, and D. Mayou, Transient localization in crystalline organic semiconductors, *Phys. Rev. B* **83**, 081202(R) (2011).
- [10] S. Ciuchi and S. Fratini, Electronic transport and quantum localization effects in organic semiconductors, *Phys. Rev. B* **86**, 245201 (2012).
- [11] A. Troisi and G. Orlandi, Dynamics of the intermolecular transfer integral in crystalline organic semiconductors, *J. Phys. Chem. A* **110**, 4065 (2006).
- [12] S. Hutsch, M. Panhans, and F. Ortmann, Charge carrier mobilities of organic semiconductors: *Ab initio* simulations with mode-specific treatment of molecular vibrations, *NPJ Comput. Mater.* **8**, 228 (2022).
- [13] T. Nematiram, D. Padula, A. Landi, and A. Troisi, On the largest possible mobility of molecular semiconductors and how to achieve it, *Adv. Funct. Mater.* **30**, 2001906 (2020).
- [14] T. Nematiram and A. Troisi, Modeling charge transport in high-mobility molecular semiconductors: Balancing electronic structure and quantum dynamics methods with the help of experiments, *J. Chem. Phys.* **152**, 190902 (2020).
- [15] D. M. Packwood, K. Oniwa, T. Jin, and N. Asao, Charge transport in organic crystals: Critical role of correlated fluctuations unveiled by analysis of Feynman diagrams, *J. Chem. Phys.* **142**, 144503 (2015).
- [16] B. Gerlach and H. Löwen, Analytical properties of polaron systems or: Do polaronic phase transitions exist or not?, *Rev. Mod. Phys.* **63**, 63 (1991).
- [17] G. Wellein and H. Fehske, Polaron band formation in the Holstein model, *Phys. Rev. B* **56**, 4513 (1997).
- [18] G. D. Filippis, V. Cataudella, A. S. Mishchenko, N. Nagaosa, A. Fierro, and A. de Candia, Crossover from super- to sub-diffusive motion and memory effects in crystalline organic semiconductors, *Phys. Rev. Lett.* **114**, 086601 (2015).
- [19] A. de Candia, G. De Filippis, L. M. Cangemi, A. S. Mishchenko, N. Nagaosa, and V. Cataudella, Two channel model for optical conductivity of high mobility organic crystals, *EPL* **125**, 47002 (2019).
- [20] Y.-C. Wang and Y. Zhao, Diagrammatic quantum Monte Carlo toward the calculation of transport properties in disordered semiconductors, *J. Chem. Phys.* **156**, 204116 (2022).
- [21] W. Li, J. Ren, and Z. Shuai, A general charge transport picture for organic semiconductors with nonlocal electron-phonon couplings, *Nat. Commun.* **12**, 4260 (2021).
- [22] H. Oberhofer, K. Reuter, and J. Blumberger, Charge transport in molecular materials: An assessment of computational methods, *Chem. Rev.* **117**, 10319 (2017).
- [23] S. Fratini, S. Ciuchi, D. Mayou, G. Trambly de Laissardière, and A. Troisi, A map of high-mobility molecular semiconductors, *Nat. Mater.* **16**, 998 (2017).

- [24] R. Blankenbecler, D. J. Scalapino, and R. L. Sugar, Monte Carlo calculations of coupled boson-fermion systems. I, *Phys. Rev. D* **24**, 2278 (1981).
- [25] S. Beyl, F. Goth, and F. F. Assaad, Revisiting the hybrid quantum Monte Carlo method for Hubbard and electron-phonon models, *Phys. Rev. B* **97**, 085144 (2017).
- [26] See the Supplemental Material at <http://link.aps.org/supplemental/10.1103/PhysRevApplied.22.L031004>, which includes Refs. [50–59], for further details, including derivations, algorithms, and simulation data.
- [27] A. S. Mishchenko, N. Nagaosa, G. De Filippis, A. de Candia, and V. Cataudella, Mobility of Holstein polaron: An unbiased approach, *Phys. Rev. Lett.* **114**, 146401 (2015).
- [28] R. Tripolt, P. Gubler, M. Ulybyshev, and L. von Smekal, Numerical analytic continuation of Euclidean data, *Comput. Phys. Commun.* **237**, 129 (2019).
- [29] M. V. Ulybyshev, C. Winterowd, and S. Zafeiropoulos, Direct detection of metal-insulator phase transitions using the modified Backus-Gilbert method, *EPJ Web. Conf.* **03008**, 175 (2018).
- [30] M. Ulybyshev, P. Buividovich, and C. Winterowd, ulybyshev/Green-Kubo\_solver: Release 1.2 (2017), used GitHub version cloned on Aug. 20, 2023.
- [31] S. Duane, A. D. Kennedy, B. J. Pendleton, and D. Roweth, Hybrid Monte Carlo, *Phys. Lett. B* **195**, 216 (1987).
- [32] P. V. Buividovich and M. I. Polikarpov, Monte-Carlo study of the electron transport properties of monolayer graphene within the tight-binding model, *Phys. Rev. B* **86**, 245117 (2012).
- [33] M. V. Ulybyshev, P. V. Buividovich, M. I. Katsnelson, and M. I. Polikarpov, Monte-Carlo study of the semimetal-insulator phase transition in monolayer graphene with realistic inter-electron interaction potential, *Phys. Rev. Lett.* **111**, 056801 (2013).
- [34] Following up on this work, we have generalized and benchmarked EFA in further detail [60].
- [35] G. G. Batrouni and R. T. Scalettar, Langevin simulations of a long-range electron-phonon model, *Phys. Rev. B* **99**, 035114 (2019).
- [36] G. G. Batrouni, G. R. Katz, A. S. Kronfeld, G. P. Lepage, B. Svetitsky, and K. G. Wilson, Langevin simulations of lattice field theories, *Phys. Rev. D* **32**, 2736 (1985).
- [37] B. Cohen-Stead, O. Bradley, C. Miles, G. Batrouni, R. Scalettar, and K. Barros, Fast and scalable quantum Monte Carlo simulations of electron-phonon models, *Phys. Rev. E* **105**, 065302 (2022).
- [38] J. Ostmeier and P. Buividovich, HMC simulations of electron-phonon systems (2024), <https://github.com/j-ostmeier/electron-phonon-hmc>.
- [39] B. Xing, W. Chiu, D. Poletti, R. T. Scalettar, and G. G. Batrouni, Quantum Monte Carlo simulations of the 2D Su-Schrieffer-Heeger model, *Phys. Rev. Lett.* **126**, 017601 (2021).
- [40] C. Feng, B. Xing, D. Poletti, R. Scalettar, and G. Batrouni, Phase diagram of the Su-Schrieffer-Heeger-Hubbard model on a square lattice, *Phys. Rev. B* **106**, 081114 (2022).
- [41] A. Götz, S. Beyl, M. Hohenadler, and F. F. Assaad, Valence-bond solid to antiferromagnet transition in the two-dimensional Su-Schrieffer-Heeger model by Langevin dynamics, *Phys. Rev. B* **105**, 085151 (2022).
- [42] X. Cai, Z. Li, and H. Yao, High-temperature superconductivity induced by the Su-Schrieffer-Heeger electron-phonon coupling, [arXiv:2308.06222](https://arxiv.org/abs/2308.06222).
- [43] S. Fratini and S. Ciuchi, Dynamical localization corrections to band transport, *Phys. Rev. Res.* **2**, 013001 (2020).
- [44] D. Vong, T. Nemataram, M. A. Dettmann, T. L. Murrey, L. S. R. Cavalcante, S. M. Gurses, D. Radhakrishnan, L. L. Daemen, J. E. Anthony, K. J. Koski, C. X. Kronawitter, A. Troisi, and A. Moulé, Quantitative hole mobility simulation and validation in substituted acenes, *J. Phys. Chem. Lett.* **13**, 5530 (2022).
- [45] C. R. Groom, I. J. Bruno, M. P. Lightfoot, and S. C. Ward, The Cambridge structural database, *Acta Cryst. B* **72**, 171 (2016).
- [46] J. E. Northrup, Two-dimensional deformation potential model of mobility in small molecule organic semiconductors, *Appl. Phys. Lett.* **99**, 062111 (2011).
- [47] H. Ishii, S. Obata, N. Niitsu, S. Watanabe, H. Goto, K. Hirose, N. Kobayashi, T. Okamoto, and J. Takeya, Charge mobility calculation of organic semiconductors without use of experimental single-crystal data, *Sci. Rep.* **10**, 2524 (2020).
- [48] S. C. B. Mannsfeld, M. L. Tang, and Z. Bao, Thin film structure of triisopropylsilylethynyl-functionalized pentacene and tetraceno[2,3-*b*]thiophene from grazing incidence x-ray diffraction, *Adv. Mater.* **23**, 127 (2011).
- [49] A. D. Scaccabarozzi, A. Basu, F. Aniés, J. Liu, O. Zapata-Arteaga, R. Warren, Y. Firdaus, M. I. Nugraha, Y. Lin, M. Campoy-Quiles, N. Koch, C. Müller, L. Tsetseris, M. Heeney, and T. D. Anthopoulos, Doping approaches for organic semiconductors, *Chem. Rev.* **122**, 4420 (2022).
- [50] L. Wang, O. V. Prezhdo, and D. Beljonne, Mixed quantum-classical dynamics for charge transport in organics, *Phys. Chem. Chem. Phys.* **17**, 12395 (2015).
- [51] I. Montvay and G. Münster, *Quantum Fields on a Lattice* (Cambridge University Press, Cambridge, 1994).
- [52] H. F. Trotter, On the product of semi-groups of operators, *Proc. Am. Math. Soc.* **10**, 545 (1959).
- [53] L. Verlet, Computer “experiments” on classical fluids. I. Thermodynamical properties of Lennard-Jones molecules, *Phys. Rev.* **159**, 98 (1967).
- [54] J. Ostmeier, Simple ways to improve discrete time evolution, *PoS LATTICE2023*, 025 (2024).
- [55] U. Wolff, and Alpha Collaboration, Monte Carlo errors with less errors, *Comput. Phys. Commun.* **156**, 143 (2004).
- [56] J. Ostmeier, Optimised Trotter decompositions for classical and quantum computing, *J. Phys. A* **56**, 285303 (2023).
- [57] I. Omelyan, I. Mryglod, and R. Folk, Symplectic analytically integrable decomposition algorithms: Classification, derivation, and application to molecular dynamics, quantum and celestial mechanics simulations, *Comput. Phys. Commun.* **151**, 272 (2003).
- [58] R. E. Peierls, Zur Theorie des Diamagnetismus von Leitungselektronen, *Z. Phys.* **80**, 763 (1933).
- [59] M. G. Endres, D. B. Kaplan, J. Lee, and A. N. Nicholson, Noise, sign problems, and statistics, *Phys. Rev. Lett.* **107**, 201601 (2011).
- [60] J. Ostmeier and P. Buividovich, Minimal autocorrelation in hybrid Monte Carlo simulations using exact Fourier acceleration, [arXiv:2404.09723](https://arxiv.org/abs/2404.09723).